High Extinction Ratio Polarization Beam Splitter Design by Low-Symmetric Photonic Crystals

Utku Gorkem Yasa, Mirbek Turduev, Ibrahim Halil Giden, and Hamza Kurt, *Member, IEEE*

***Abstract*—A novel concept of polarization beam splitting with high polarization extinction ratio is proposed based on the polarization sensitive self-collimation feature of symmetry reduced photonic crystals. The idea utilizes self-collimation mechanism and rotated isofrequency contours arising due to the deliberately implemented symmetry reduction in the photonic structure. Square lattice of low-symmetric rectangular air holes in dielectric background are numerically analyzed in both frequency and time domains. The operating bandwidth of the device is $\Delta\lambda = 53$ nm. At $\lambda = 1.55$ μm, polarization extinction ratios are $\sim$23 and $\sim$18 dB for transverse electric and transverse magnetic ports, respectively. The investigated device is 46.4 μm $\times$ 12.4 μm in size and based on a uniform, planar, and homogenous structure. Therefore, there is no need for an additional splitting assistance to separate the two orthogonal polarizations. Possible fabrication imperfections are also analyzed and it is observed that polarization extinction ratios stay above 17 dB when error percentage is around 5.5%. With having these advantages, symmetry reduced photonic crystal-based polarization beam splitters can be a good candidate for optical communication applications.**

***Index Terms*—Photonic crystals, photonic integrated circuits, polarization beam splitters, self-collimation.**

I. Introduction

PHOTONIC crystals (PCs) are periodic structures that have been studied since their first introduction to the literature in 1987 [1], [2]. At first, they were designed to achieve complete photonic band gaps (PBGs) which block the flow of photons in specific frequency ranges in all propagation directions. After several years, researchers have exploited new significant features of PCs such as self-collimation [3], [4], super-prism effect [5], negative refraction [6], and flat focusing mirrors [7] such that the ability to manipulate light without structural defects has been shown to be feasible differently from a PBG based light management.

Manuscript received October 29, 2016; revised January 4, 2017; accepted January 22, 2017. Date of publication January 24, 2017; date of current version April 20, 2017. The work of U. G. Yasa and I. H. Giden was supported by the Scientific and Technological Research Council of Turkey (TUBITAK) under Project 115R036. The work of H. Kurt was supported in part by the Scientific and Technological Research Council of Turkey (TUBITAK) under Project 115R036 and in part by Turkish Academy of Sciences.

U. G. Yasa, I. H. Giden, and H. Kurt are with the TOBB University of Economics and Technology, Ankara 06560, Turkey (e-mail: gorkemyasa@etu.edu.tr; igiden@etu.edu.tr; hkurt@etu.edu.tr).

M. Turduev is with the TED University, Ankara 06420, Turkey (e-mail: mirbek.turduev@tedu.edu.tr).

Color versions of one or more of the figures in this paper are available online at http://ieeexplore.ieee.org.

Digital Object Identifier 10.1109/JLT.2017.2657697

Polarization beam splitters (PBSs) are very essential components in photonic integrated circuits (PICs) and optical communications (polarization-division-multiplexing) due to the capability of separating two orthogonal polarizations, i.e., transverse magnetic (TM) and transverse electric (TE) into different propagation directions. Most of the photonic devices are designed to operate properly under one type of polarization. Hence, if the incident light is unpolarized or partially polarized then it is imperative to split the wave into two orthogonal polarizations. Earlier PBS devices [8]–[12] were not sufficiently compact in terms of dimensions to meet optical circuit requirements because of being on the order of millimeters. In contrast with the conventional ones, PBSs that are made of PCs are more compact and efficient. Various PBS devices based on PCs have been introduced in the literature [13]–[18]. To briefly exemplify some pioneering PBS studies, Ao *et al.* suggested splitting of polarization based on the negative refraction for one type of polarization and conventional refraction for the other one [15]. The weakness of the negative refraction concept is the strong diffraction of light (beam spreading) after the refraction occurs at the air-PC interface. Another drawback could be the requirement of oblique excitation targeting the relevant section of the iso-frequency contours (IFCs). Other concept of polarization splitting with PCs was introduced by Ohtera *et al.* that uses PBGs to filter two different polarizations [16]. In addition to that, PBG effect was combined with self-collimation feature to polarize self-guiding waves with a splitting band gap region [17]. Such type of PC heterostructures may suffer from the inclusion of the defect region (splitting region) inside the periodic structure so that possible fabrication errors may lead to weakening or shifting of the gaps. An alternative method was proposed by Wu *et al.* that utilizes differential dispersion characteristics of TM and TE modes in order to separate the polarization states [18]. This type of PBS concept suffers from strong light diffraction and low transmission for both polarizations because of the absence of self-collimation phenomenon.

Aside from the methods mentioned above, here we propose a new concept of PBS with high polarization extinction ratios (PERs) by reducing the structural symmetry of PC unit-cells in a periodic medium. Inclusion of additional PC rods or modifications in the unit-cell scale (e.g., switching circular rods with elliptical ones) give rise to low-symmetric PC structures with broken rotational symmetry [19]. Although most of the PC related studies have focused on circular and square shaped unit-cell elements, low-symmetric PC media has recently gathered a great attention because of their capabilities to control light

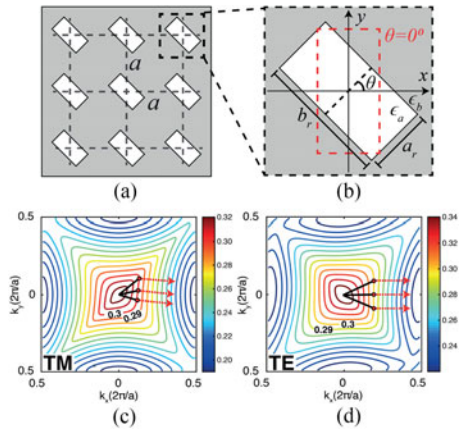

Fig. 1. (a) Square lattice of 2D rectangular air holes. (b) Geometric representation of 2D unit-cell with $a_r = 0.30a$, $b_r = 0.60a$, $\epsilon_a = 1$ and $\epsilon_b = 9.61$. 2nd band IFC plot of (c) TM and (d) TE polarization states, respectively. In both IFC figures, frequencies that correspond to operational bandwidth are emphasized with bold fonts. Direction of gradient vectors for normalized frequency $a/\lambda = 0.300$ is shown with red arrows.

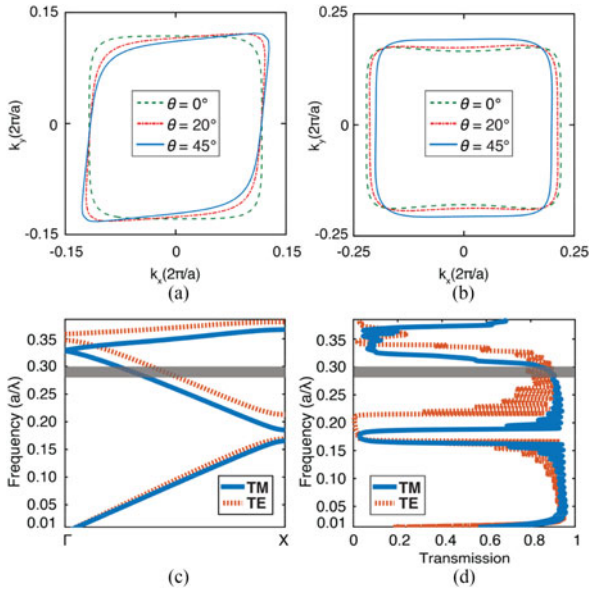

Fig. 2. Influence of air hole angular orientation on IFCs is shown for normalized frequency a/λ = 0.300 with respect to θ parameter for (a) TM and (b) TE polarizations. (c) Band structure for both polarizations and (d) corresponding transmission spectrum when $\theta = 45°$. In (c) and (d), gray shaded field indicates the operating frequency interval ($a/\lambda = 0.290 - 0.300$) of the designed PBS device.

propagation in different ways such as tilted self-collimation and focusing [20], [21], diffraction-free light propagation [22], and wavelength division demultiplexing [23].

II. Design Approach and Principle of Operation

In this study, the proposed low-symmetric PC that utilizes tilted self-collimation feature to split polarizations consists of square lattice rectangular PC air holes with a fixed lattice constant $a = 460$ nm as depicted in Fig. 1(a). Permittivity value of the dielectric background and air holes are taken to be $\epsilon_b = 9.61$ and $\epsilon_a = 1$, respectively. Fig. 1(b) shows a zoomed view of each PC air hole geometry in a dielectric background with size parameters equal to $a_r = 0.30a$ and $b_r = 0.60a$. Angular orientation of each unit-cell element is denoted by the angle θ with respect to x-axis as shown in Fig. 1(b).

The geometry of the PC unit-cell provides the construction of complex photonic structures that may yield distinct spectral features [19]. IFCs are created to investigate the propagation behavior of light through the proposed PC structure. These contours give us information about dispersive characteristics of the structure and the underlying physical mechanism of polarization splitting phenomena. The propagation of light within the PC structure can be defined by the formula, $\vec{v}_g(x, y) = \nabla_k \omega(k)$, where $\vec{v}_g$ is the group velocity of light and k is the wave vector. Furthermore, $\vec{v}_g$ represents the direction of energy flow which is perpendicular to the dispersion contours. In other words, the propagating beam follows the direction which is determined by the IFCs.

Plane wave expansion method is performed in order to extract the dispersion characteristics of the PC structure [24]. As it is well known, 1st bands of TM and TE polarizations of square lattice PC structures consist of circular shaped IFCs (isotropic medium) and this feature is generally independent of the unit-cell structure. On the other hand, 2nd bands of both polarizations may contain square-like shaped IFCs which imply the existence of a conventional self-collimation phenomenon [3], [4]. Self-collimated beam paves the way for diffraction limited propagation of light within the PC medium with high transmission efficiency. This characteristic makes PC structures that utilize self-collimation effect more attractive rather than using additional assistant structures to convey the light efficiently. Low-symmetric PCs can efficiently manipulate the shape of self-collimated IFCs and they lead to a tilted self-collimation effect [20], [21], [23]. Therefore, for PBS design, the 2nd bands of TE and TM polarization modes were considered. In this study, we have calculated IFCs of the 2nd TM and TE polarization bands for the rotation angle of $\theta = 45°$ which can be seen in Figs. 1(c) and (d), respectively. The reason to select 45° will be explained later in the text. In Fig. 1(c), one can observe tilted square-shaped dispersion curves with tilted flatness along the Γ-X direction for TM polarization mode. This flatness leads to the generation of tilted self-collimating beams inside PC structure along the directions normal to these flat curves (directions of light shown with red arrow as insets). On the other hand, in case of TE modes, the rotation of the rectangular air holes does not give rise to rotation of square-shaped dispersion curves. Therefore, one can observe conventional self-collimation effect in the Γ-X direction. It can be deduced that the orientation of the rectangular air holes in dielectric background has stronger influences on the direction of light propagation inside the medium for TM polarization compared to TE polarization case. Thus, operating at both TE and TM polarization modes within those tilted and normal self-collimation regimes paves the way to design a PBS structure for a certain bandwidth.

Figs. 2(a) and (b) are collection of dispersion curves when θ traces values from 0° to 45° in counterclockwise direction. Different frequency contours are chosen at fixed operating

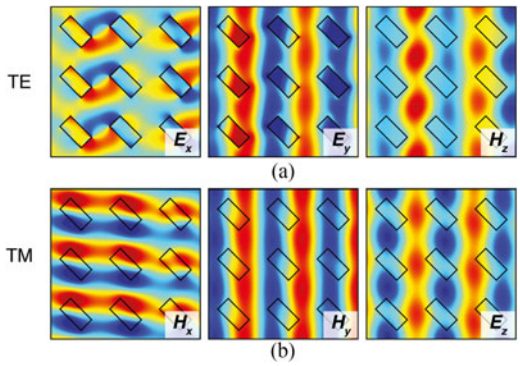

Fig. 3. Electric (E) and magnetic (H) field distributions of (a) TE (E_x, E_y, H_z) and (b) TM (H_x, H_y, E_z) polarized modes at normalized frequency $a/\lambda = 0.295$ when $\theta = 45°$.

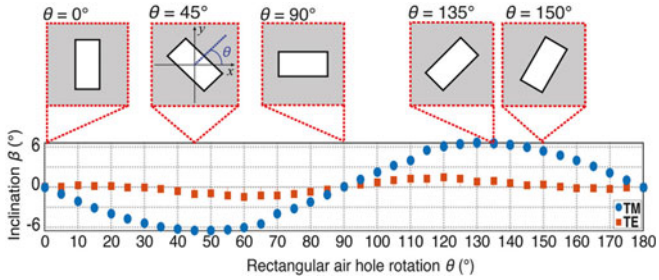

Fig. 4. Impact of rectangular air hole rotation (θ) on the contour inclination angles of both TM (β_{TM}) and TE (β_{TE}) polarization states at normalized frequency $\mathrm{a}/\lambda = 0.300$. When $\theta = 45°$, inclination angles equal to $\beta_{\mathrm{TM}} = 6.507°$ and $\beta_{\mathrm{TE}} = 0.983°$ for TM and TE polarizations, respectively.

frequency of $a/\lambda = 0.300$ for TM and TE modes, respectively. As can be deduced from these figures, an increase in the angle θ directly affects the TM curves by transforming their square-like shapes to the tilted ones without deforming the flatness of the dispersion curves as shown in Fig. 2(a). Inclination of the 2nd TM band IFCs gives rise to a tilted self-collimating effect and the tilt amount can be tuned by only adjusting the air hole rotation angle θ. On the other hand, TE curves are not influenced much with different orientations of rectangular PC holes but flat region of 2nd band IFC gets slightly enlarged, i.e., k_y-width of self-collimation region slightly increases. Therefore, one can deduce that light beam with different TM and TE polarizations can follow different paths (directions) inside the periodic structure due to the above mentioned self-collimating effects. This property enables the polarization splitting of the incident light beams at the output of the structure.

TE and TM modes act differently for the orientation of the symmetry reduced unit element of PCs within the selected operating bandwidth. The difference can be linked with the mode energy distributions and slope of the bands. When we plot the electric field component (E_z) of TM states and magnetic field component (H_z) of TE states at normalized frequency of $a/\lambda = 0.295$ and $\theta = 45°$, different field distributions can be seen, as shown in Figs. 3(a) and (b), respectively. As can be observed from Fig. 3(b), mode energy for TM polarization is concentrated at the corners of the rectangular holes that are closest whereas the same types of energy profiles plotted for TE case in Fig. 3(a) indicate that field concentrates at the distant corners of the air holes. Consequently, TM polarization becomes more sensitive to the orientation of the unit-cell element and IFCs of TM states turn out to be tilted compared to TE polarization ones. The orientation sensitivity of TM polarization can also be associated with the dispersion diagram as represented in Fig. 2(c). The selected normalized frequency is close to the TM band edge at the Γ point compared to the TE mode that has larger slope. It is known that small group velocity indicates the presence of slow light propagation. As a result, strong light interaction with the structured material is expected. This can explain the sensitive response of TM mode for the orientation of rectangular holes.

Fig. 4 shows the dependence of contour inclination angles β_{TM} for TM polarization (indicated as blue colored circular markers) and β_{TE} for TE polarization (indicated as orange colored square markers) states with respect to the angular orientation θ of the rectangular air holes. The corresponding figure also shows the visual representation of air hole orientation cases which corresponds to specific θ values of an $a \times a$ unit-cell element. In order to calculate the inclination angles (β_{TM} and β_{TE}) within the interested frequency region, gradient of scalar IFC distributions was obtained numerically for different θ unit-cell rotation angles. Extracted gradient vector fields show the propagation direction of light and by measuring the angle between gradient vector and the reference k_{x}-axis ($k_y = 0$), inclination angles were calculated in the vicinity of $a/\lambda = 0.300$ contour lines. Inclination variation of TM contour curves gives a sinusoidal response while tracing θ parameter from 0° to 180° in counterclockwise direction and β_{TM} takes its maximum value at $\theta = 45°$. Differently from TM polarization, TE contours are not affected much by the rotation of rectangular air holes and β_{TE} almost equals to 0° where small changes can be ignored comparing to β_{TM}. While changing the orientation of individual PC cell, the highest polarization separation angle has been obtained when the orientation angle of PC unit-cell element lies within the interval of $\theta = 40° - 50°$. When $\theta = 45°$, β_{TE} and β_{TM} values are equal to 6.507° and 0.983°, respectively, as indicated in Fig. 4. For angles larger (or lower) than $\theta = 45°$, it is observed that the obliqueness in TM IFC curves reverts back to its square-like shape [see Fig. 2(a)] which can be confirmed by the sinusoidal changing manner of the TM inclination angle β_{TM} in Fig. 4. In accordance with these results, we fixed the unit-cell element orientation angle for our PBS device as $\theta = 45°$ to achieve the highest polarization splitting performance.

The inspection of the band diagrams allows the identification of modal characteristic of the propagating light. The designed structure operates as a single mode in the Γ-X propagation direction for both TM and TE polarizations at the 2nd bands in the operating frequency intervals $a/\lambda = 0.185 - 0.320$ and $a/\lambda = 0.213 - 0.347$, respectively, see Fig. 2(c). Thus, the modal dispersion due to multi-mode propagation within the same interval is inhibited. Since, we are inspecting polarization splitting behavior of the PC structure, transmission amount of light as high as possible is desired. For this reason,

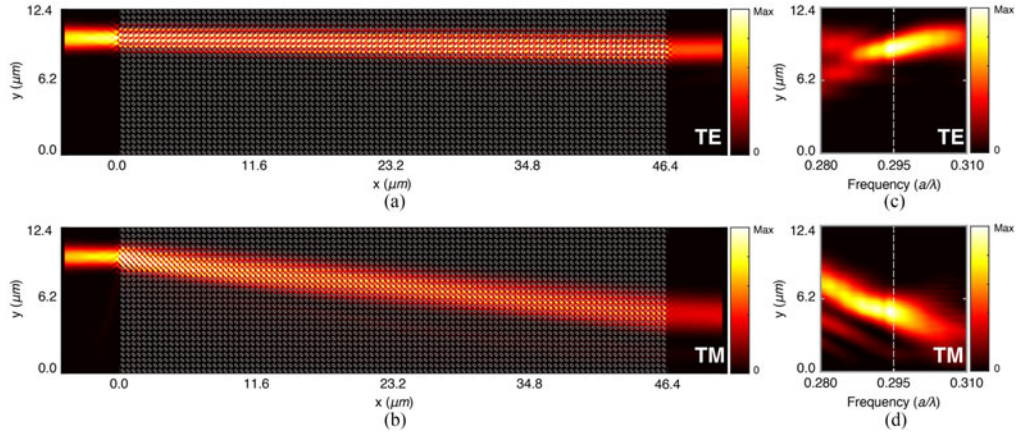

Fig. 5. Spatial intensity distributions for (a) TE and (b) TM polarizations at the normalized frequency $a/\lambda = 0.295$. Intensity with respect to different normalized frequencies of (c) TE and (d) TM polarization states at the output ports of the proposed structure. Dashed white lines in (c) and (d) indicate the intensity distribution at normalized frequency $a/\lambda = 0.295$.

transmission coefficients of the simple low-symmetric PC (without introducing input and output ports) for both polarizations are calculated by using finite-difference time-domain method [25] and represented in Fig. 2(d). As can be observed from Fig. 2(d), at self-collimating frequencies, high transmission efficiencies over 70% are obtained for both TM and TE modes without any help of an index-matched intermediate layer. Nevertheless, proper anti-reflection coating structures [26], [27] can be placed at the input/output interfaces of PC layer in order to stabilize the performance of the proposed device by reducing Fabry-Pérot oscillations at the operating frequency interval.

III. Discussion: Evaluation of Numerical Results

Time domain calculations have been employed in order to investigate the polarization splitting feature in our proposed low-symmetric PC device. Computational domain is surrounded by perfectly matched layers in order to eliminate back reflections and the mesh size is fixed to $\Delta x = \Delta y = a/32$. The dimensions of the low-symmetric PC based PBS configuration is set to be $[\mathrm{L}_x, \mathrm{L}_y] = [46.4\ \mu\mathrm{m}, 12.4\ \mu\mathrm{m}]$. The designed PBS structure is excited with a continuous source with spatial size of 3.68 μm operating at normalized frequency of $a/\lambda = 0.295$ and the corresponding spatial intensity field distributions for both TE and TM polarizations are represented in Fig. 5(a) and (b), respectively. Because of the tilted self-collimation phenomenon in TM polarization, a beam spatial shifting in the lateral y-direction emerges inside the PBS structure as shown in Fig. 5(b). On the other hand, the incident beam propagates straight along x-direction with near zero diffraction due to emerged conventional self-collimation effect at the 2nd band of TE polarization, see Fig. 5(a). These conditions provide spatial separation of incident beams into two different polarizations at the output of the low-symmetric PC structure.

To better estimate the channel arrangements for the polarization splitting application, the vertical field intensity cross-sections of output beams are superimposed for different incident sources operating at frequencies between $a/\lambda = 0.280 - 0.310$ for both TE and TM polarizations as shown in Figs. 5(c) and (d),

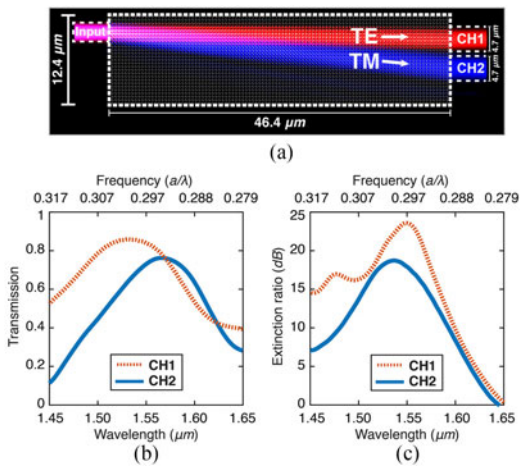

Fig. 6. (a) Operational diagram of the proposed PBS device with output channels CH1 and CH2. (b) Transmission efficiencies at CH1 (TE-port) and CH2 (TM-port). (c) PER curves at the CH1 and CH2 ports.

respectively. As can be clearly observed from these figures, the incident beam almost directly propagates inside the PBS within the frequency range of $a/\lambda = 0.288 - 0.305$ for TE polarization [Fig. 5(c)] whereas deflection of the incident beam occurs and lateral shift increases for TM polarization as the frequency increase from $a/\lambda = 0.286$ to $a/\lambda = 0.300$, see Fig. 5(d).

Output channel transmissions as well as extinction ratios should be in adequate level for efficient PBS applications. The designed low-symmetric PBS structure is excited by an unpolarized Gaussian pulse centered at the wavelength of 1.550 μm with a bandwidth of 0.20 μm. Due to inherent dispersive characteristics of the proposed PBS system, TE and TM polarizations are being divided while propagating through the PC medium so that a channel separation for different polarizations is achieved at the output ports, as can be seen by the spatial intensity distribution provided in Fig. 6(a). The upper and lower adjacent output channels are denoted as channel-1 (CH1) and channel-2 (CH2) with the same widths of 4.7 μm and channel spacing is 1.23 μm between them. The calculated transmissions as well

as extinction ratios for TE and TM polarizations are plotted via dashed-red and solid-blue lines, respectively in Figs. 6(b) and 6(c). In Fig. 6(b), transmission efficiency curves are calculated between the wavelengths of $\lambda = 1.450 - 1.650\,\mu$m with their equivalent normalized frequency values from $a/\lambda = 0.279$ to $a/\lambda = 0.317$. The polarization splitting feature of the proposed device covers the wavelength interval of $\lambda = 1.533 - 1.586\,\mu$m with an operating bandwidth of 53 nm. As it can be seen from the same figure, in the range of optical C-band wavelengths (1.530–1.565 μm), maximum transmission efficiency at the CH1 port exceeds 85% and for the CH2 port it moves beyond 76%. Thus, the results show that the proposed PBS device has an acceptable transmission value to use in optical communication applications. Moreover, the transmission values for both channels can be increased by exploiting a suitable index-matching layer to the entry and exit surfaces of the PBS device as a further development.

Aside from the transmission efficiency described above (also known as insertion loss), isolation of polarization states is another important factor that greatly affects the performance of a PBS photonic device. PER can be defined as a ratio of the output transmissions between the desired and unwanted polarization states at an output channel. The PERs at each output channel of the presented device are calculated in dB scale by the following equation.

$$\mathrm{PER_{CH\#}} = 10\log_{10}\frac{\mathrm{T_{desired}}}{\mathrm{T_{unwanted}}}, \tag{1}$$

where, $\mathrm{T_{desired}}$ is output transmission of the requested polarization state and $\mathrm{T_{unwanted}}$ is output transmission of the unwanted polarization state at a channel. For example, if we want to calculate the PER curve at CH1, $\mathrm{T_{desired}}$ and $\mathrm{T_{unwanted}}$ variables turn into transmission efficiencies of TE and TM polarized light, respectively. In Fig. 6(c), extinction ratio curves at the output of CH1 (dashed-red) and CH2 (solid-blue) are plotted within the wavelength interval of 1.450–1.650 μm and corresponding normalized frequency values are shown as in Fig. 6(b). In the C-band range, the results indicate that $\mathrm{PER_{CH1}}$ and $\mathrm{PER_{CH2}}$ values are greater than 21.01 dB and 16.00 dB, respectively. At $\lambda = 1.550\,\mu$m, $\mathrm{PER_{CH1}} = 23.64$ dB, $\mathrm{PER_{CH2}} = 18.00$ dB and the transmission efficiencies are 84% and 73%, respectively, which means that this homogenous PBS design may be utilized in silicon PICs for optical communication applications.

Apart from the proposed PC structure, additional calculations were conducted for PC unit-cells with different geometries in order to determine their polarization splitting capability. It is concluded from the performed numerical calculations that the polarization splitting characteristic can be obtained from C_2 symmetric PCs with any geometries such as elliptic, crescent, concentric and rhombic PCs. Nevertheless, the best case among the inspected ones is observed for the rectangular PCs case in terms of polarization splitting performance (TE and TM separation), which was the reason for choosing rectangular PC unit cell for PBS application.

Robustness of the proposed PBS concept is another important factor and it should be analyzed in case of structural imperfections which can be caused by possible fabrication defects/errors.

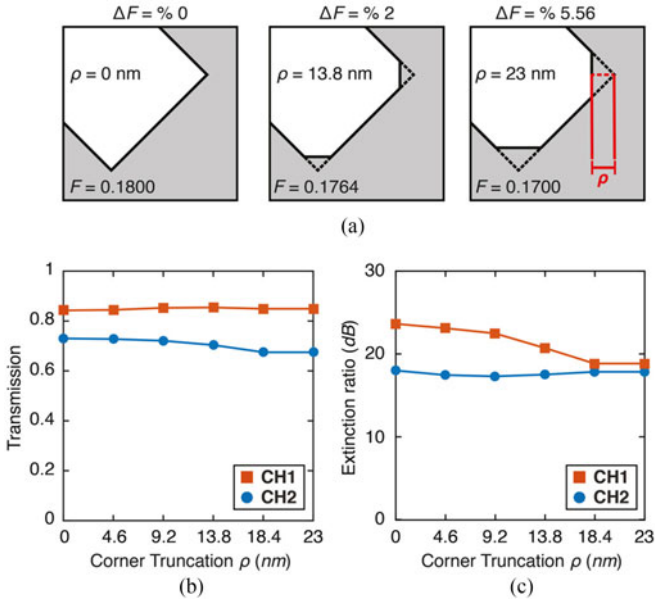

Fig. 7. (a) Visual explanation of corner truncation ρ and close-up representations of two imperfection states ($\rho = 13.8$ nm, $\rho = 23$ nm) and a perfect fabrication case ($\rho = 0$ nm). Resultant filling ratios (F) and their percentage changes (ΔF) are also included. Impact of corner truncation on (b) transmission efficiencies and (c) PER values are plotted for output ports CH1 and CH2 at $\lambda = 1.550\,\mu$m.

In general, perfectly sharpened corners of unit-cell elements (e.g., rectangular shaped rods or holes) are difficult to produce which require precise and high-resolution fabrication process. Aside from the fabrication technique, maintaining the sharpness of these shapes is another challenging point that may affect the operational characteristic of the device adversely. To analyze the durability of the proposed PBS structure within this scope, rectangular air holes of the unit-cells are deformed purposely to mimic fabrication and usage imperfections by introducing some level of truncation amount ρ to the sharp inside corners of air holes. Fig. 7(a) shows two selected visual representations of these corner deformations and a perfect fabrication case (when $\rho = 0$) together with corresponding air filling ratios (F) and percentage change in filling ratios (ΔF). Here ΔF parameter can also be assumed as an error percentage because it shows filling area alterations of rectangular air holes and indicates the percentage of error in terms of the structural filling. In order to check the polarization splitting performance of the proposed device, transmission efficiencies and PER values are measured in each 4.6 nm step of ρ parameter until it equals to 23 nm. Fig. 7(b) represents the impact of imperfections on transmission at CH1 (TE) and CH2 (TM) output ports of the device when $\lambda = 1.550\,\mu$m. The given graph demonstrates that transmittance at each exit port does not change much with the increase of structural deformation factor. For instance when we truncate the corners of rectangular air holes by $\rho = 13.8$ nm as represented in Fig. 7(a), air filling ratio reduces by $\Delta F = 2\%$ with a resultant value of $F = 0.1764$. In this condition, CH1 transmission covers its value around %84 while the transmission at CH2 drops from 72.87% to %70.23 at $\lambda = 1.550\,\mu$m. For the other case in the same figure, truncation is raised to

$\rho = 23$ nm with an increased value of $\Delta F = 5.5\%$ ($F = 0.1700$). Therefore, transmission efficiency of CH1 maintains its value above %84 while CH2 declines to 67.35%. These results show that the PBS design is robust enough in terms of the transmission performance although the structure is exposed to high level of error percentages (e.g., $\Delta F = 5.5\%$) comparing to the perfect case. Aside from transmission efficiency, imperfection influence on PER values is another criterion that determines the durability of polarization isolation at output ports of the PBS device. For this reason, relation between the structural deformations and PER values at each output channels is plotted in Fig. 7(c) for $\lambda = 1.550\,\mu$m. Given figure shows that truncating corners and consequently reducing the *F* factor induces degradation in $\mathrm{PER_{CH1}}$ and $\mathrm{PER_{CH2}}$ values as expected. For instance, when fabrication error percentage is $\Delta F = 5.5\%$ ($\rho = 23$ nm) with reduced filling ratio of $F = 0.1700$, $\mathrm{PER_{CH1}}$ decreases from 23.64 dB to 18.84 dB while $\mathrm{PER_{CH2}}$ is exposed to a reduction from 18 dB to 17.84 dB. According to these findings, it is revealed that PERs stay above 17 dB at both output ports even if the fabrication error ratio reaches high levels like 5.5%. As a result, one can conclude that the above given investigations indicate that proposed PBS configuration is robust to possible fabrication imperfections. Furthermore, the proposed PBS device is feasible with precise dimensions by the help of state-of-art SOI technology [28].

In the design and fabrication processes, selection of dielectric material is an important step for photonic devices. Although the utilized material in the PBS device has a dielectric constant of $\epsilon_b = 9.61$, different materials with higher refractive index (e.g., $\epsilon_b = 12$) such as Si may also be used as an alternative background medium because low-symmetric PC configurations still maintain their anomalous dispersion properties even for different composing materials. This property indicates that the operating principle of the proposed device is robust to permittivity change. Thus, different materials with interested transparent spectral intervals can be utilized to design the proposed PBS device.

It is also essential for the proposed self-collimation based PBS concept to compare with other polarization splitting models in terms of the performance and structure properties. Recent approaches in PBS designs are mainly focused on directional couplers (DCs) [29]–[36], ring resonators [37], [38], multimode interference couplers [39], [40], band-gap feature of PCs [41] and pixel based devices [42]. Among them, DC configuration is the most common concept that is used to separate beams into two orthogonal polarizations by utilizing different coupling lengths for TM and TE polarization states. However, DC based PBS structures are mostly lack of polarization isolation at output ports because of the close interaction between two adjacent waveguides. On the other hand, the presented PBS structure is a non-DC device and one can easily isolate distinct polarizations due to diffraction free light propagation inside photonic medium. To the best of the authors' knowledge, the tilted self-collimation effect is exploited for the first time in PBS realization. We should note that conventional (non-tilted) self-collimation based other PBS devices exist in the literature and they should be analyzed to compare with our presented concept. Previous studies that based on conventional self-collimation [17], [43]–[45] are in need of additional band-gap structures (to reflect back one polarization and transmit the other one through exit ports) because conventional self-collimation is incapable of polarization splitting when it is used as stand-alone. Necessity of reflective structures makes these PBS devices more challenging in design and production processes because of the structural non-uniformity and requirements to find suitable band-gap materials in desired frequencies. Furthermore, possible fabrication imperfections in these additional structures affect their band-gap characteristics adversely. Therefore, performance of these devices is decreased due to deformed periodicity of the assistant band-gap materials. On the other hand, the proposed low-symmetric PBS device does not need a splitting assistance because polarization separation ability originates from its own dispersion relation and therefore structure remains uniform in fabrication and usage processes. Moreover, nonuse of reflection interface has another advantage that output beams are in the same horizontal direction whereas conventional self-collimation based PBS devices split two polarizations into different directions. This property makes low-symmetric PBS configuration feasible and easy-to-use while integrating devices to the photonic circuit.

IV. Conclusion

In conclusion, we have proposed and numerically demonstrated a novel concept of PBS photonic device by using the polarization sensitive self-collimation behavior of low-symmetric PCs. The designed structure is $46.4\,\mu\text{m} \times 12.4\,\mu$m in size and made of all-dielectric homogenous periodic medium which separates two orthogonally polarized modes with its own unique dispersion property. Moreover, the designed PBS device does not need additional splitting assistance or any line defect in order to control the propagation direction of polarized beams inside the structure. Due to the self-guidance of light inside the structure, high PERs are obtained for both TM and TE polarization states at the optical communication wavelengths. At $\lambda = 1.550\,\mu$m, TE (TM) port has an acceptable transmission efficiency 84.1% (72.87%) with high PER around 23.64 dB (18 dB) and operating bandwidth is 53 nm. With these advantages, low-symmetric PC based PBSs can be used in many applications which require the separation of light polarizations.

References

[1] E. Yablonovitch, "Inhibited spontaneous emission in solid-state physics and electronics," *Phys. Rev. Lett.*, vol. 58, no. 20, pp. 2059–2062, 1987.

[2] S. John, "Strong localization of photons in certain disordered dielectric superlattices," *Phys. Rev. Lett.*, vol. 58, no. 23, pp. 2486–2489, 1987.

[3] H. Kosaka *et al.*, "Self-collimating phenomena in photonic crystals," *Appl. Phys. Lett.*, vol. 74, no. 9, pp. 1212–1214, 1999.

[4] J. Witzens, M. Lončar, and A. Scherer, "Self-collimation in planar photonic crystals," *IEEE J. Sel. Topics Quantum Electron.*, vol. 8, no. 6, pp. 1246–1257, Nov./Dec. 2002.

[5] H. Kosaka *et al.*, "Superprism phenomena in photonic crystals: toward microscale lightwave circuits," *J. Lightw. Technol.*, vol. 17, no. 11, pp. 2032–2038, Nov. 1999.

[6] B. Momeni *et al.*, "Compact wavelength demultiplexing using focusing negative index photonic crystal superprisms," *Opt. Express.*, vol. 14, no. 6, pp. 2413–2422, 2006.

[7] Y. C. Cheng *et al.*, "Flat focusing mirror," *Sci. Rep.*, vol. 4, 2014, Art. no. 6326.

[8] P. Albrecht, M. Hamacher, H. Heidrich, D. Hoffmann, H. P. Nolting, and C. M. Weinert, "TE/TM mode splitters on InGaAsP/InP," *IEEE Photon. Technol. Lett.*, vol. 2, no. 2, pp. 114–115, Feb. 1990.

[9] J. J. G. M. van der Tol, J. W. Pedersen, E. G. Metaal, Y. S. Oei, H. van Brug, and I. Moerman, "Mode evolution type polarization splitter on InGaAsP/InP," *IEEE Photon. Technol. Lett.*, vol. 5, no. 12, pp. 1412–1414, Dec. 1993.

[10] R. M. de Ridder, A. F. M. Sander, A. Driessen, and J. H. J. Fluitman, "An integrated optic adiabatic TE/TM mode splitter on silicon," *J. Lightw. Technol.*, vol. 11, no. 11, pp. 1806–1811, Nov. 1993.

[11] L. B. Soldano, A. H. de Vreede, M. K. Smit, B. H. Verbeek, and F. H. Groen, "Mach-Zehnder interferometer polarization splitter in InGaAsP/InP," *IEEE Photon. Technol. Lett.*, vol. 6, no. 3, pp. 402–405, Mar. 1994.

[12] H. Maruyama, M. Haruna, and H. Nishihara, "TE-TM mode splitter using directional coupling between heterogeneous waveguides in $LiNbO_3$," *J. Lightw. Technol.*, vol. 13, no. 7, pp. 1550–1554, Jul. 1995.

[13] E. Schonbrun, Q. Wu, W. Park, T. Yamashita, and C. J. Summers, "Polarization beam splitter based on a photonic crystal heterostructure," *Opt. Lett.*, vol. 31, no. 21, pp. 3104–3106, 2006.

[14] J. Hou, L. Wang, C. Yang, B. Wang, and S. Chen, "Compact high extinction ratio asymmetric polarization beam splitter of periodic rods waveguide," *Appl. Opt.*, vol. 54, no. 34, pp. 10277–10282, 2015.

[15] X. Ao, L. Liu, L. Wosinski, and S. He, "Polarization beam splitter based on a two-dimensional photonic crystal of pillar type," *Appl. Phys. Lett.*, vol. 89, no. 17, 2006, Art. no. 171115.

[16] Y. Ohtera, T. Sato, T. Kawashima, T. Tamamura, and S. Kawakami, "Photonic crystal polarisation splitters," *Electron. Lett.*, vol. 35, no. 15, pp. 1271–1272, 1999.

[17] V. Zabelin *et al.*, "Self-collimating photonic crystal polarization beam splitter," *Opt. Lett.*, vol. 32, no. 5, pp. 530–532, 2007.

[18] L. Wu, M. Mazilu, J.-F. Gallet, T. F. Krauss, A. Jugessur, and R. M. De La Rue, "Planar photonic crystal polarization splitter," *Opt. Lett.*, vol. 29, no. 14, p. 1620–1622, 2004.

[19] I. H. Giden, M. Turduev, and H. Kurt, "Reduced symmetry and analogy to chirality in periodic dielectric media," *J. Eur. Opt. Soc.—Rapid Publications*, vol. 9, 2014, Art. no. 14045i.

[20] H. Kurt, M. Turduev, and I. H. Giden, "Crescent shaped dielectric periodic structure for light manipulation," *Opt. Express*, vol. 20, no. 7, pp. 7184–7194, 2012.

[21] M. Turduev, I. H. Giden, and H. Kurt, "Modified annular photonic crystals with enhanced dispersion relations: Polarization insensitive self-collimation and nanophotonic wire waveguide designs," *J. Opt. Soc. Amer. B*, vol. 29, no. 7, pp. 1589–1598, 2012.

[22] I. H. Giden, M. Turduev, and H. Kurt, "Broadband super-collimation with low-symmetric photonic crystal," *Photon. Nanostruct. Fundam. Appl.*, vol. 11, no. 2, pp. 132–138, 2013.

[23] M. Turduev, I. H. Giden, and H. Kurt, "Extraordinary wavelength dependence of self-collimation effect in photonic crystal with low structural symmetry," *Photon. Nanostruct. Fundam. Appl.*, vol. 11, no. 3, pp. 241–252, 2013.

[24] S. Johnson and J. D. Joannopoulos, "Block-iterative frequency-domain methods for maxwell's equations in a planewave basis," *Opt. Express*, vol. 8, no. 3, pp. 173–190, 2001.

[25] A. F. Oskooi, D. Roundy, M. Ibanescu, P. Bermel, J. D. Joannopoulos, and S. G. Johnson, "Meep: A flexible free-software package for electromagnetic simulations by the FDTD method," *Comput. Phys. Commun.*, vol. 181, no. 3, pp. 687–702, 2010.

[26] S. Lee, J. Choi, J. Kim, H. Y. Park, and C. Kee, "Reflection minimization at two-dimensional photonic crystal interfaces," *Opt. Express*, vol. 16, no. 6, pp. 4270–4277, 2008.

[27] B. Momeni and A. Adibi, "Adiabatic matching stage for coupling of light to extended bloch modes of photonic crystals," *Appl. Phys. Lett.*, vol. 87, no. 17, pp. 1–3, 2005.

[28] E. Kuramochi, H. Taniyama, T. Tanabe, K. Kawasaki, Y. G. Roh, and M. Notomi, "Ultrahigh-Q one-dimensional photonic crystal nanocavities with modulated mode-gap barriers on SiO2 claddings and on air claddings," *Opt. Express*, vol. 18, no. 15, pp. 15859–15869, 2010.

[29] K. Zhou *et al.*, "A novel polarizer based on directional coupler and surface plasmon polaritons," *Optoelectron. Lett.*, vol. 9, no. 6, pp. 430–433, 2013.

[30] Y. Ma, G. Farrell, Y. Semenova, H. P. Chan, H. Zhang, and Q. Wu, "Low loss, high extinction ration and ultra-compact plasmonic polarization beam splitter," *IEEE Photon. Technol. Lett.*, vol. 26, no. 7, pp. 660–663, Apr. 2014.

[31] T. Uematsu, T. Kitayama, Y. Ishizaka, and K. Saitoh, "Ultra-broadband silicon-wire polarization beam combiner/splitter based on a wavelength insensitive coupler with a point-symmetrical configuration," *IEEE Photon. J.*, vol. 6, no. 1, pp. 1–8, Feb. 2014.

[32] J. Hou, L. Wang, C. Yang, B. Wang, and S. Chen, "Compact high extinction ratio asymmetric polarization beam splitter of periodic rods waveguide," *Appl. Opt.*, vol. 54, no. 34, 2015, Art. no. 10277.

[33] S. Chen, H. Wu, and D. Dai, "High extinction-ratio compact polarisation beam splitter on silicon," *Electron. Lett.*, vol. 52, no. 12, pp. 1043–1045, 2016.

[34] P. Rani, Y. Kalra, and R. K. Sinha, "Complete photonic bandgap-based polarization splitter on silicon-on-insulator platform," *J. Nanophoton.*, vol. 10, no. 2, 2016, Art. no. 26023.

[35] T. Zhang, X. Yin, L. Chen, and X. Li, "Ultra-compact polarization beam splitter utilizing a graphene-based asymmetrical directional coupler," *Opt. Lett.*, vol. 41, no. 2, p. 356, 2016.

[36] S. Gao, S. Member, Y. Wang, S. Member, and K. Wang, "Low-loss and broadband 2×2 polarization beam splitter based on silicon nitride platform," *IEEE Photon. Technol. Lett.*, vol. 28, no. 18, pp. 1936–1939, Sep. 2016.

[37] X. Xu *et al.*, "Polarization beam splitter based on honeycomb-lattice photonic crystal ring resonators," *J. Mod. Opt.*, vol. 61, no. 5, pp. 373–378, 2014.

[38] S. Zhu *et al.*, "Tunable polarization beam splitter based on optofluidic ring resonator," *Opt. Express*, vol. 24, no. 15, pp. 17511–17521, 2016.

[39] M. Yin, W. Yang, Y. Li, X. Wang, and H. Li, "CMOS-compatible and fabrication-tolerant MMI-based polarization beam splitter," *Opt. Commun.*, vol. 335, pp. 48–52, 2015.

[40] X. Sun, M. Z. Alam, J. S. Aitchison, and M. Mojahedi, "Compact and broadband polarization beam splitter based on a silicon nitride augmented low-index guiding structure," *Opt. Lett.*, vol. 41, no. 1, pp. 163–166, 2016.

[41] T. Wang *et al.*, "Design and verification of the polarization beamsplitter based on photonic crystals," *Opt. Commun.*, vol. 351, pp. 40–44, 2015.

[42] B. Shen, P. Wang, R. Polson, and R. Menon, "An integrated-nanophotonics polarization beamsplitter with $2.4 \times 2.4\ \mu m^2$ footprint," *Nature Photon.*, vol. 9, no. 6, pp. 378–382, 2015.

[43] J.-M. Park, S.-G. Lee, H.-R. Park, and M.-H. Lee, "High-efficiency polarization beam splitter based on a self-collimating photonic crystal," *J. Opt. Soc. Amer. B*, vol. 27, no. 11, pp. 2247–2254, 2010.

[44] X. Chen *et al.*, "Polarization beam splitter based on photonic crystal self-collimation Mach-Zehnder interferometer," *Opt. Commun.*, vol. 284, no. 1, pp. 490–493, 2011.

[45] X. Shen, K. Han, Y. Shen, H. Li, Y. Wu, and G. Tang, "Dispersion-based all photonic crystals polarization beam splitter," *Phys. Lett. A*, vol. 369, no. 5/6, pp. 524–527, 2007.

Authors' biographies not available at the time of publication.